Results in Engineering 25 (2025) 103970

Contents lists available at ScienceDirect

Results in Engineering

journal homepage: www.sciencedirect.com/journal/results-in-engineering

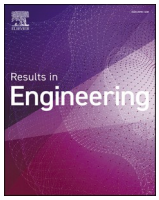

Research paper

Isotherm and kinetic models of SO_2 adsorption on palm kernel shell-activated carbon and xerogel blends: Effect of flow rate and contact time

Ali Mohamed Saleh [a,b], Azil Bahari Alias [a], Syed Shatir A. Syed Hasan [a], Ali H. Jawad [c,d,e], Thaer Abdulwahhab Shihab [f], Obed M. Ali [g,*], Wan Azlina Wan Ab Karim Ghani [h], Hadi Hamdi Mahdi [a], Noah Mohammed Saleh [b,i], Omer Khalil Ahmed [b]

[a] School of Chemical Engineering, College of Engineering, Universiti Technologi MARA, Shah Alam 40450, Malaysia
[b] Renewable Energy Research Unit, Alhawija Institute, Northern Technical University, Mosul 41002, Iraq
[c] Faculty of Applied Sciences, Universiti Teknologi MARA, 40450 Shah Alam, Selangor, Malaysia
[d] Advanced Biomaterials and Carbon Development Research (ABCD) Group, Faculty of Applied Sciences, Universiti Teknologi MARA, 40450 Shah Alam, Selangor, Malaysia
[e] Environmental and Atmospheric Sciences Research Group, Scientific Research Center, Al-Ayen University, Thi-Qar, Nasiriyah 64001, Iraq
[f] Technical Engineering College, Al-Bayan University, Baghdad, Iraq
[g] College of Oil and Gas Engineering Techniques, Northern Technical University, Mosul 41002, Iraq
[h] Sustainable Process Engineering Research Centre (SPERC), Faculty of Engineering, Universiti Putra Malaysia, Serdang 43400, Malaysia
[i] Faculty of Mechanical Engineering University of Tabriz, Iran

ARTICLE INFO

Keywords:
Adsorbents
Pollutant
Thomas model
Yoon-Nelson model
Adam-Bohart model
Pseudo-first and second order models

ABSTRACT

Sulphur dioxide (SO_2) is released into the atmosphere when coal-fired power plants run, which may substantially impair the environment. SO_2 in flue gas causes respiratory difficulties and acid rain, and as energy consumption rises, the amount of SO_2 emitted into the environment also rises. SO_2 can effectively be removed from gases or air streams through adsorption, where it is captured and retained onto a solid surface, such as activated carbon. This research focuses on developing and evaluating a composite adsorbent made from palm kernel shell-activated carbon and xerogel (PKSACX) for the adsorption of sulphur dioxide (SO_2). The main objectives are to study the modelling of adsorption isotherm (Thomas, Yoon-Nelson, and Adam-Bohart models) and to determine the adsorption kinetics (pseudo-first and pseudo-second order) of the performance of SO_2 adsorption on a blended series of palm kernel shell-activated carbon and xerogel. Based on the result obtained, the adsorption process mathematically described by the Thomas and Yoon-Nelson Model is the best model for SO_2 removal compared to the Adam-Bohart model. Pseudo-First Order and Pseudo-Second Order kinetic models were utilized. The correlation coefficient (R^2) was used to assess the equation's suitability. The PKSACXB adsorption processes suit both the pseudo-first and pseudo-second order equations. This indicates that throughout the adsorption process, both physisorption and chemisorption occur.

1. Introduction

Sulphur dioxide (SO_2) is one of the pollutants in the atmosphere that is mainly emitted from the processing of fossil fuels or industrial activity, endangering the environment and human health [1,2]. The maximum allowable concentration of sulphur dioxide (SO_2) in the air over a year is (0.03–0.04) ppm for it to be considered safe for human health and the environment [3]. Brief contact with SO_2 can damage the human respiratory system, causing breathing difficulties, especially for individuals with asthma, notably children, who are more vulnerable to its effects [4,5]. The release of SO_2 that results in elevated levels of this gas in the atmosphere also triggers the production of various sulphur oxides (SO_x) [6]. These SO_x compounds can interact with other substances in the air, forming tiny particles. These particles are part of particulate matter (PM) pollution, capable of deeply infiltrating the lungs and, in significant amounts, posing health risks [7]. Besides affecting health, SO_2 also contributes to acid deposition in the environment, leading to

* Corresponding author.
E-mail address: obedmajeed@gmail.com (O.M. Ali).

https://doi.org/10.1016/j.rineng.2025.103970
Received 1 November 2024; Received in revised form 31 December 2024; Accepted 3 January 2025
Available online 5 January 2025

Nomenclature

SO_2	Sulphur Dioxide
SO_x	sulphur oxides
FGD	flue gas desulphurization
GDL	Glucono delta-lactone
mm	Millimeter
g	Gram
ppm	Part per million
PM	particulate matter
C_o	Initial concentration
C_f	Final concentration
$CaCO_3$	Calcium carbonate
t	Time (min)
m	Mass of adsorbent
F	Flow rate (L/hr)
PFO	Pseudo-First Order
PSO	Pseudo-Second Order
AIC	Akaike Information Criterion
AC	Activated Carbon
PKS	Palm kernel shell Biochar
PKSAC	Palm kernel shell-activated carbon
PKSACX	Palm kernel shell-activated carbon Xerogel
PKSACXB	Palm kernel shell-activated carbon Xerogel Blended
K_{TH}	Thomas rate constant
K_{YN}	Yoon-Nelson proportionality constant
K_{AB}	Adam-Bohart kinetics constant
τ	Time required for retaining 50 % of the initial adsorbate in min
N_o	Maximum volumetric sorption capacity in mg/L
V	linear flow rate in cm/min.
q_o	The initial amount of SO_2
q_t	Amount of SO_2 adsorbed at time t (mg/g)
q_e	Amount of SO_2 adsorbed at equilibrium (mg/g)
R^2	Coefficient of correlation

the acidification of lakes and streams, as well as harming tree foliage and agricultural crops [8]. Transforming organic waste into absorbent and sustainable materials has become increasingly crucial for both environmental protection and public health [9]. Numerous researchers conduct a characterization of the initial adsorbent before the adsorption process [10]. This study examines the adsorption kinetics and identifies the equilibrium isotherm that best fits the adsorption process [11–13]. Adsorption isotherms are used to mathematically model adsorption processes, allowing for the simulation of adsorption behavior without conducting experiments [14,15]. Numerous methods exist for minimizing sulphur emissions, including flue gas desulphurization (FGD), coal washing, cleaner fuel sulphur recovery units, and biological approaches.

In industries relying on coal as a fuel source, Sulphur, typically present as pyrite (Fe_2S), can be conveniently eliminated through coal washing with water. However, operational costs and efficiency issues may offset this process due to alterations in fuel properties. Flue gas desulphurization (FGD) stands out as the primary method employed at an industrial scale to address SO_2 issues, primarily due to its straightforward process and remarkable desulfurization capacity, reaching over 99 % with wet sorbent [16]. Dry adsorption desulfurization methods commonly employ natural or synthetic zeolites, activated carbons, and metal oxides as their primary adsorbents. This method captures Sulphur and diminishes the release of other pollutants like SO_3 and mercury into the environment. These materials exhibit crystalline or amorphous structures at macro and nanoscales, and they can undergo modifications to enhance their physicochemical properties, thereby improving their adsorption capacity for specific molecules. Activated carbon is frequently utilized as an adsorbent packed into absorbers due to its strong attraction for adsorbing various hazardous gases at low concentrations (below 0.3–0.25 %). This is owed to its expansive surface area, intricate pore structure, and hydrophobic characteristics. Its excellent adsorption capabilities and chemical stability render it a highly effective pollutant adsorbent. Activated carbon can be derived from diverse raw materials, with bio-waste often being a preferred source due to the substantial volume generated [17]. Previously, lignocellulose precursors or biomass such as palm kernel, wood, coconut shells, rice husks, and other lignocellulose materials were carbonized to generate porous activated carbons.

In this work, the adsorption of SO_2 using blended as a solid adsorbent was investigated and aligned with [18,19]. Carbonizing dry organic gels typically activates the resultant biochar to further improve its porous structure [20]. During the removal of SO_2 using activated carbon, the gas is separated from the flue gas through adsorption. Subsequently, the adsorbed SO_2 undergoes catalytic oxidation, facilitated by oxygen and water vapor, transforming into sulfuric acid. This resulting sulfuric acid is then stored within the pores of the activated carbon [21]. Carbon gels, distinctive porous carbon substances characterized by their low bulk density, elevated electrical conductivity, hierarchical pore arrangement, and substantial specific surface area, find extensive applications in energy storage, catalysis, supercapacitors, and adsorption, among other uses. The creation of carbon gels can be achieved through various drying methods. When derived from aqueous organic gels, these are known as aerogels, xerogels, or Cryogel, distinguished by the specific drying technique employed [22]. Numerous recent studies have leveraged nanomaterials to enhance outcomes across various domains, including engineering, medicine, and environmental applications, in laboratory research and practical implementations [23–26]. There are explicitly identifying the limitations of current methods, such as the high costs, scalability issues for fossil fuel consumption, and limited efficiency of conventional adsorbents like zeolites and standalone activated carbon [27]. We highlighted the research exploring the synergistic benefits of combining palm kernel shell-activated carbon with xerogel, which leverages the former's adsorption efficiency and the latter's unique physicochemical properties [28]. This study aims to enhance the SO_2 adsorption process by investigating the adsorption isotherm and kinetic behavior of a novel blended series of Palm Kernel Shell-Activated Carbon and Xerogel. Building on previous research that highlighted carbon xerogels' remarkable adsorption capabilities and performance, this study aims to optimize the material blend for improved SO_2 removal efficiency.

2. Materials and methods

A cylinder containing 50 ppm of SO_2, balanced with nitrogen, was used throughout this experiment to evaluate the adsorption capabilities of three adsorbents: PKSAC, PKSACX, and PKSACXB. The SO_2 gas was sourced from Alpha Gas Solution Sdn. Bhd, Malaysia. PKSAC, sourced from Kuala Korai, Kelantan, 18,000, Malaysia, was utilized as the raw material for preparing xerogel (PKSACX). Calcium carbonate ($CaCO_3$), sodium alginate, and glucono-δ-lactone (GDL) were supplied by the College of Engineering, School of Chemical Engineering. Distilled water was used as the solvent for the Xerogel synthesis. The methodology solely encompasses investigations into adsorption isotherms and adsorption kinetics. The adsorption tests were performed using a multilayer adsorption column with three levels of adsorption trays; each tray's inner diameter 1.85 inches, and the height 3 inches. Due to hazardous gases, stainless steel was used for the column's construction.

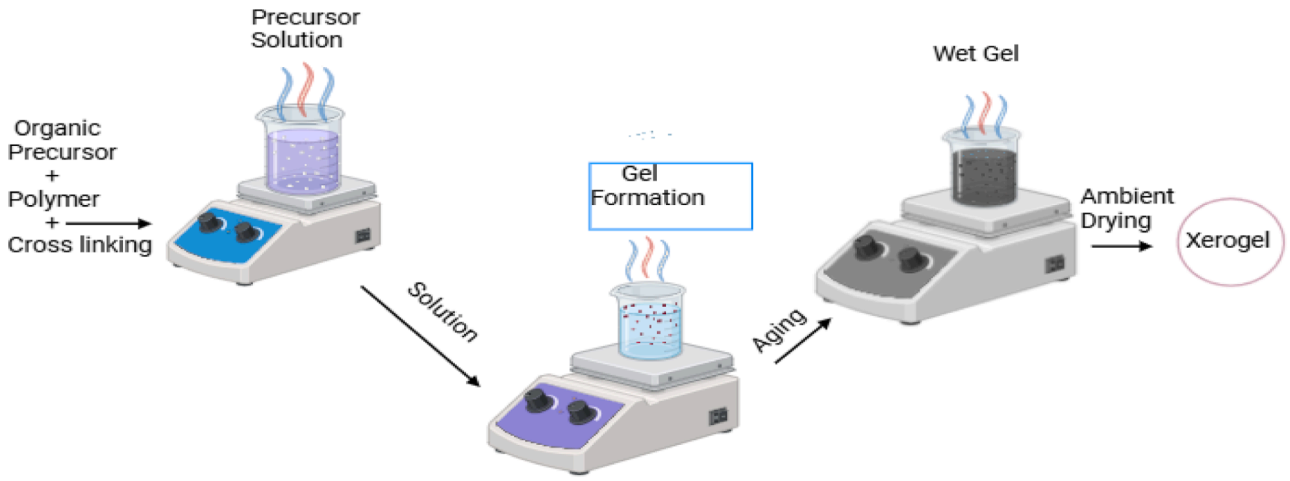

Fig. 1. Shows the main steps of Xerogel preparation.

2.1. Preparation of PKSACX

In this experiment, palm kernel shell-activated carbon was chosen as the organic raw material and purchased from the market; the synthesis and characterization of all materials used in this study were done in previous paper research by Ali and Hadi [22]. Palm kernel shell-activated carbon (PKSAC) served as the raw material for xerogel production. The PKSAC was crushed using a mortar and pestle to achieve 1 to 2 mm particle sizes. A total of 2.88 g of crushed PKSAC was used for the xerogel preparation. The sol-gel method was employed, comprising three main steps—sol preparation, gelation, and drying—. First, 4.13 g of sodium alginate was dissolved in 500 mL of distilled water with magnetic stirring until a homogeneous solution was formed. Next, 1.73 g of calcium carbonate and 2.88 g of PKSAC were added to the solution. Gelation commenced by adding 4.58 g of glucono delta-lactone (GDL) to the mixture, leading to hydrogel formation. The hydrogel was then transferred to a square mold and cooled at 4 °C until gelation was complete. Finally, the hydrogel was removed from the mold, placed on an aluminum tray, and prepared for the drying process [22]. Fig. 1 shows the main steps of xerogel preparation to improve the adsorption properties. Xerogel, known for its porous structure and high surface area—was incorporated alongside palm kernel shell-activated carbon in the experimental setup. The xerogel was synthesized using sodium alginate, calcium carbonate, and glucono delta lactone as the key components. Throughout the experiment, an SO_2 concentration of 50 ppm was used to assess the adsorption capabilities of PKSACX.

Xerogel drying was carried out using oven drying, a solvent removal process that aids in transforming hydrogel into xerogel. The hydrogel sample was subjected to an extended drying period at a controlled low temperature of 60 °C in an oven. This procedure was conducted over three days to ensure effective solvent removal and maintain the structural integrity of the xerogel [29].

2.2. Characterization procedure

The characterization of palm kernel shell biochar (PKS), palm kernel shell activated carbon (PKSAC), and palm kernel shell activated carbon Xerogel (PKSACX) was performed using multiple analytical techniques and we obtained the following. In elemental analysis (CHNS-O), the samples were degassed at 90 °C for 1 hour, followed by an additional 4 h at 300 °C under a nitrogen (N_2) atmosphere. (N_2) adsorption and desorption isotherms were achieved at 77 K, following the procedure by [30]. Brunauer-Emmett-Teller (BET) surface area was measured using a Micrometrics 3Flex automatic surface analyzer. Approximately 0.1–0.2 g of each sample was analyzed, heating at a rate of 10 °C/min. The process utilized (N_2) adsorption and desorption at a 10 mL/min flow rate and was conducted at 40 °C for 6 h. Fourier Transform Infrared Spectroscopy (FTIR) analysis, following ASTM E1252–98 standards, was performed using a Perkin Elmer Spectrum 2000 FTIR spectrometer. The structural composition changes were examined over a wavelength range of 4000 to 500 cm^{-1}). X-ray Diffraction (XRD) analysis was employed to investigate the morphological and crystalline structure of the samples. Thermogravimetric Analysis (TGA) was conducted to evaluate the thermal stability of the materials, following ASTM standard D5142–02a. This comprehensive characterization provided insights into the physical, chemical, and structural properties of PKS, PKSAC, and PKSACX.

2.3. Methods

The adsorption test was conducted using a fixed-bed column where the concentration of SO_2 was the focus parameter. This study aimed to determine the optimal adsorption conditions concerning flow rate in equilibrium and kinetic studies. The experiment involved varying the flow rate and contact time while keeping all other parameters constant as the weight of the adsorbent, temperature, and pressure. Our experiments with other gases, such as H_2S, revealed that temperature and pressure inversely affect adsorption efficiency. Furthermore, previous studies indicate that the best effective weight of the adsorbent at a concentration of 50 ppm is 20 gs [19,31]. The gas flow rate was investigated as a parameter in the equilibrium studies. To evaluate its impact, experiments were conducted at different gas flow rates of 100 L/h, 200 L/h, and 300 L/h. During these experiments, the inlet concentration was maintained at 50 ppm of sulfur dioxide (SO_2), and the adsorption process was carried out over 30 min. The exit concentration was recorded every minute throughout the experiment. While examining the effect of the gas flow rate, the adsorbent mass was kept constant at 20 g, the gas temperature was set to ambient conditions, and the gas pressure was maintained at 1 bar In a previous study on hydrogen sulfate adsorption using xerogel as an adsorbent, we found that temperature and pressure adversely affected pollutant adsorption. As a result, these variables were excluded from consideration in this study [19,32,33].

2.3.1. Adsorption isotherm

At equilibrium and constant temperature, the adsorption isotherm depicts the connection between the adsorbate in the surrounding phase and the adsorbate adsorbed on the adsorbent's surface. In general, isotherm data are connected using several isotherm models, with the best-fitting model used for analyzing adsorption behavior [34]. The models used were the Thomas, Adams-Bohart, and Yoon-Nelson models, and various parameters were developed from each model to explain the adsorption column's performance. The linear adsorption models are shown below [18,35].

Table 1
Elemental analysis of PKSB, PKSAC, and PKSBX.

Raw materials	C %	H %	N %	S %	O %
PKS	43.2	1.36	0.36	0.51	54.57
PKSAC	45.6	1.21	0.14	0.31	52.74
PKSACX	44.4	3.55	0.51	0.50	51.04

Table 2
Data of pore size distribution and specific surface area.

Materials	Specific surface area (m^2/g)	Pore volume (cm^3/g)	Pore size (nm)
PKS	299.7565	0.376	2.17783
PKSAC	802.175	0.1632	1.87716
PKSACX	2.6359	0.0109	16.52524

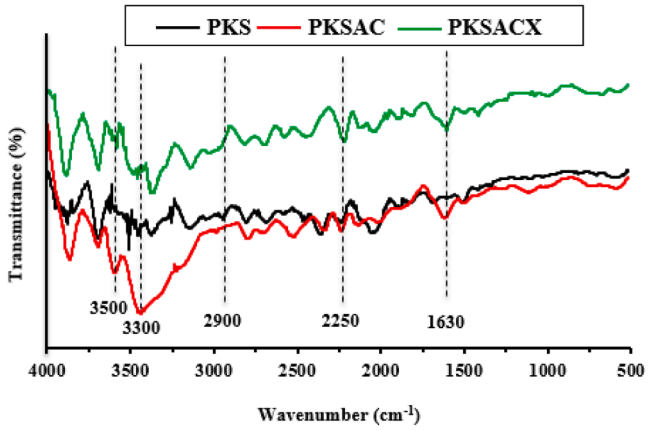

Fig. 2. FTIR spectrum of PKS, PKSAC, and PKSACX.

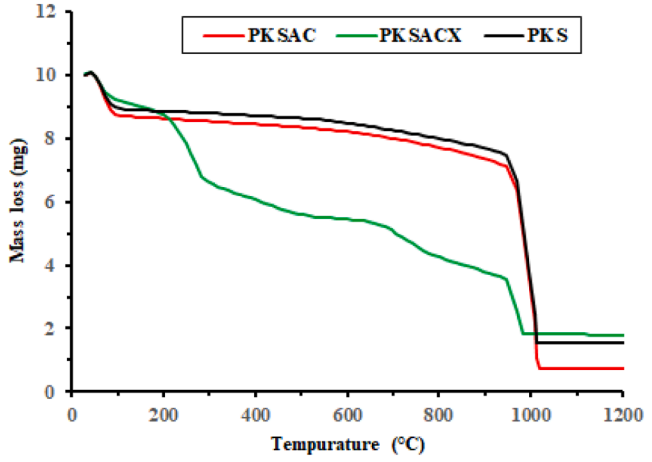

Fig. 3. TGA curves of PKS, PKSAC, and PKSACX.

Linear Thomas model eq. (1):

$$In\left(\frac{C_o}{C_f}-1\right)=\frac{(k_{TH}q_o m)}{F}\ (k_{TH}C_o t) \quad (1)$$

where K_{TH} is the Thomas rate constant in L/min.mg and q_o is the maximum concentration of SO_2 in mg/g.

Linear Yoon- Nelson model eq. (2):

$$In\left(\frac{C_f}{C_o-C_f}\right)=k_{YN}(t-\tau) \quad (2)$$

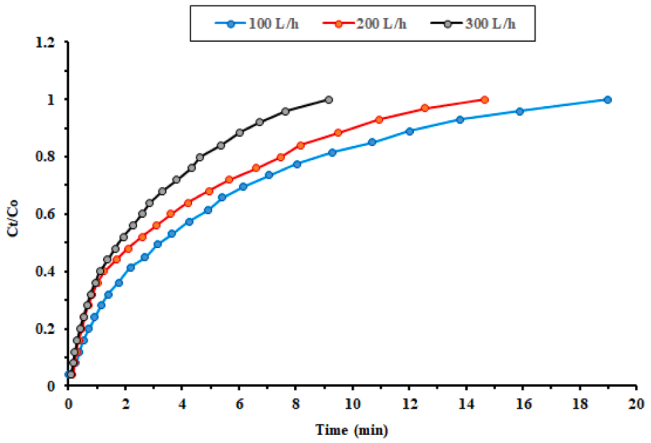

Fig. 4. Effect of gas flow rates (100 L/h, 200 L/h, and 300 L/h) on PKSACXB.

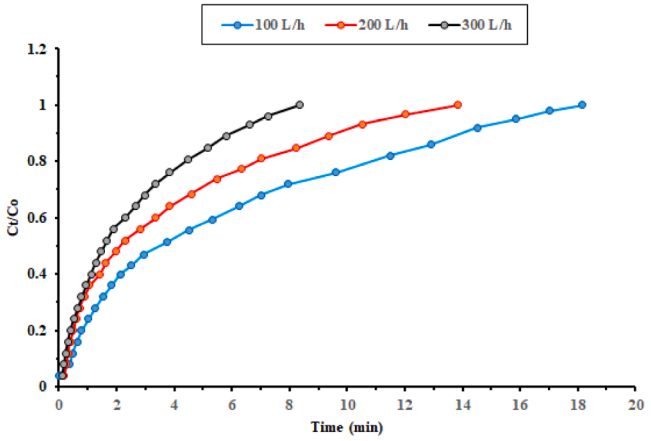

Fig. 5. Effect of gas flow rates (100 L/h, 200 L/h, and 300 L/h) on PKSACX.

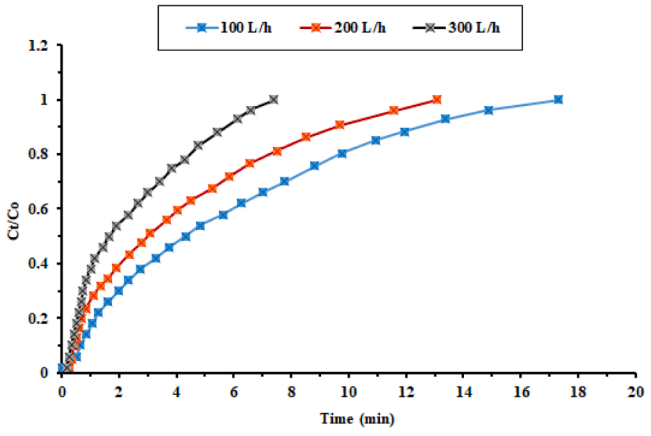

Fig. 6. Effect of gas flow rates (100 L/h, 200 L/h, and 300 L/h) on PKSAC.

where: K_{YN} is the Yoon -Nelson proportionality constant in min^{-1} and τ is the time required for retaining 50 % of the initial adsorbate in min

Linear Adam-Bohart model eq. (3):

$$In\left(\frac{C_f}{C_o}\right)=k_{AB}C_o t-\frac{(k_{AB}N_o V)}{F} \quad (3)$$

where: K_{AB} is the Adam-Bohart kinetics constant in l/mg, No is the maximum volumetric sorption capacity in mg/L and V is the linear flow

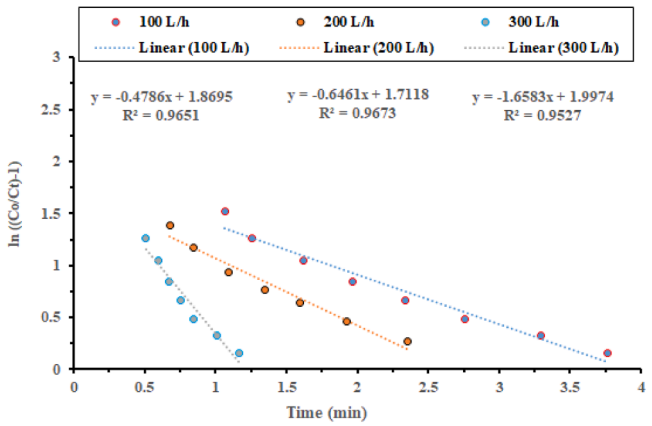

Fig. 7. Effect of Different Flowrate for Thomas Model PKSAC.

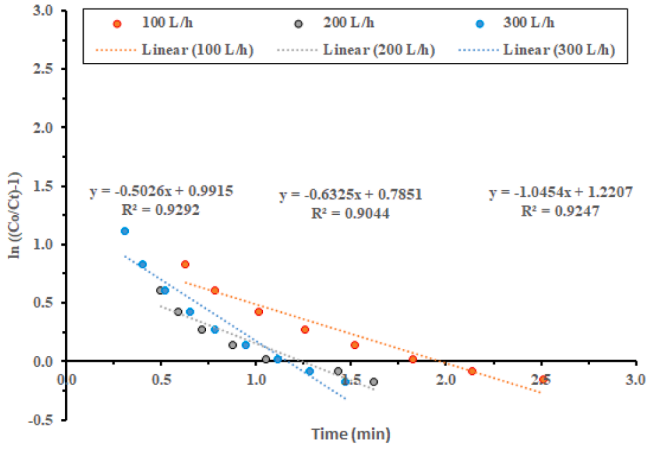

Fig. 8. Effect of Different Flowrate for Thomas Model PKSACX.

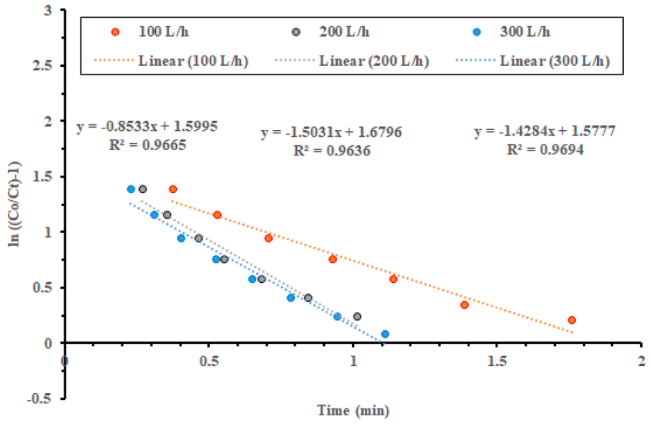

Fig. 9. Effect of Different Flowrate for Thomas Model PKSACXB.

rate in cm/min.

2.3.2. Kinetic studies

Pseudo-first and pseudo-second-order rate laws are often used to simulate adsorption kinetics. The pseudo-first-order kinetic equation and pseudo-second-order kinetic equation are provided below [18,36].

The linearization will yield the equation as shown below:

Pseudo-first order eq. (4):

$$In\ (q_e - q_t) = In\ q_e - kt \tag{4}$$

Pseudo-second order eq. (5):

$$\frac{t}{q_t} = \frac{1}{q_e} + \frac{1}{k_2 q_e^2} \tag{5}$$

where q_t is the amount of SO_2 adsorbed at time t (mg/g). q_o is the initial amount of SO_2 adsorbed and is zero for fresh adsorbent. q_e is the amount of SO_2 adsorbed at equilibrium (mg/g).

The data is used to plot the aforementioned isotherm models, and the kinetic equation with the highest coefficient of correlation (R^2) is chosen as the isotherm model best suited for mathematically recreating the adsorption process.

3. Result and discussion

3.1. Physicochemical properties

3.1.1. Elemental analysis

The Perkin Elmer PE2400 Elemental Analyzer was utilized to conduct the comprehensive examination of carbon (C), hydrogen (H), nitrogen (N), sulfur (S), and oxygen (O) CHNS-O elements. The elemental analysis of PKS, PKSAC, and PKSACX is described in Table 1. Based on the results, all samples have high carbon and oxygen content. PKSAC has a higher carbon content than PKS and PKSACX; it depends on activation temperature. Increasing temperature activation increases carbon content due to the discharge of volatile matter. Throughout this process, chemical reactions may occur, which might cause the removal of functional groups containing carbon or organic constituents. Consequently, this decreases the overall carbon content with an increase in oxygen content as shown in Table 1. These results will help to improve adsorption capacity.

3.1.2. Brunauer-Emmett teller theory (BET)

The BET method was utilized to characterize the specific surface area (m^2/g), pore volume (m^3/g), and average pore size (nm) of PKS, PKSAC and PKSACX. After mixing several chemicals, the volume and pore size increased when PKS undergoes gelation. The BET analysis results for PKSACX reflect the effect of using chemicals with a fixed formulation, specifically 4.13 g of sodium alginate, 1.73 g of calcium carbonate, and 4.58 g of GDL for the internal gelation process. Additionally, increasing the ratio to 1:10 affects the results. These chemical quantities were obtained by [37]. The BET surface area of PKSACX measured 2.6359 m^2/g, indicating relatively lower values than those of PKS and PKSAC 299.7565 and 802.178, respectively. When classifying pores based on their diameters in the context of physisorption, pores with widths ranging approximately 50–100 nm (0.05 μm) are termed macropores, those within the range of 2 nm to 50 nm are referred to as mesopores, and pores not surpassing about 2 nm in width are categorized as micropores as listed in Table 2 [38].

3.1.3. Fourier transform infrared spectroscopy (FTIR)

Fourier transform infrared (FTIR) spectroscopy was utilized to identify and analyze alterations in functional groups of PKS, PKSAC, and PKSACX. Fig. 2 depicts the FTIR spectra of PKSB, PKSAC, and PKSX. Fig. 2 shows peaks inside the O—H stretching area. The obtained spectra show significant and wide peaks at 3546.82 cm^{-1} for PKS, 3528.45 cm^{-1} for PKSAC, and 3513.76 cm^{-1} for PKSACX, suggesting the occurrence of O—H stretching. The peak mentioned earlier was recognized as the specific frequency of a hydrogen-bonded hydroxyl group (O—H), with the peak down within the range of wave numbers 3550 to 3200 cm^{-1}. The observed phenomenon suggests the existence of alcohols, which can be linked to the absorption of H_2O on the surfaces of PKS, PKSAC, and PKSACX. The vibration caused by the stretching of the C—H bond was seen at a wavenumber of 2921.17 cm^{-1} for PKS, 2901.53 cm^{-1} for PKSAC, and in the range of 2851.73 cm^{-1} was observed for the PKSACX. Similar results were noticed during the study [38]. The observed band at

Table 3
Thomas Adsorption Isotherm Model.

Type of Adsorbent	F (L/h)	W (g)	R^2	Slope	Interception at y-axis	Equation	K_{TH} (L/min.mg)	q_o (mg/g)
PKSAC	100	20 g	0.9651	−0.4786	1.8695	$y = -0.4786x + 1.8695$	0.00957	976.546
	200	20 g	0.9673	−0.6461	1.7118	$y = -0.6461x + 1.7118$	0.01292	824.71
	300	20 g	0.9527	−1.6583	1.9974	$y = -1.6583x + 1.9974$	0.03316	703.364
PKSACX	100	20 g	0.9247	−1.0454	1.2207	$y = -1.0454x + 1.2207$	0.02090	291.921
	200	20 g	0.9044	−0.6325	0.7851	$y = -0.6325x + 0.7851$	0.01265	620.632
	300	20 g	0.9247	−1.0454	1.2207	$y = -1.0454x + 1.2207$	0.02090	875.765
PKSACXB	100	20 g	0.9665	−0.8533	1.5995	$y = -0.8533x + 1.5995$	0.01706	468.621
	200	20 g	0.9636	−1.5031	2.0122	$y = -1.5031x + 1.6796$	0.03006	669.35
	300	20 g	0.9694	−1.4284	1.5777	$y = -1.4284x + 1.5777$	0.02856	928.391

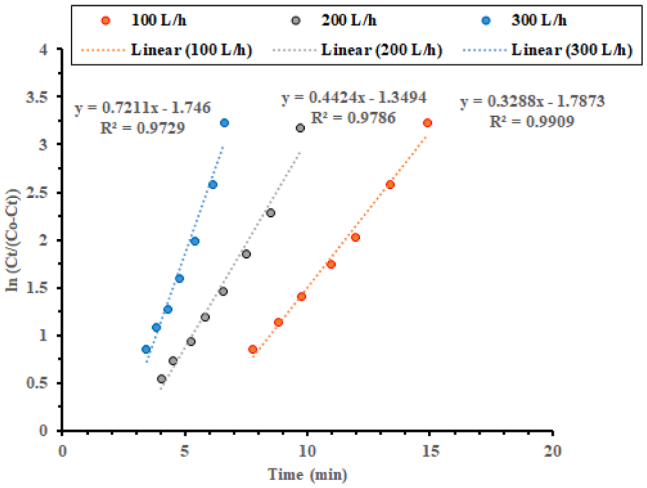

Fig. 10. Effect of Different Flowrate for Yoon Nelson Model PKSAC.

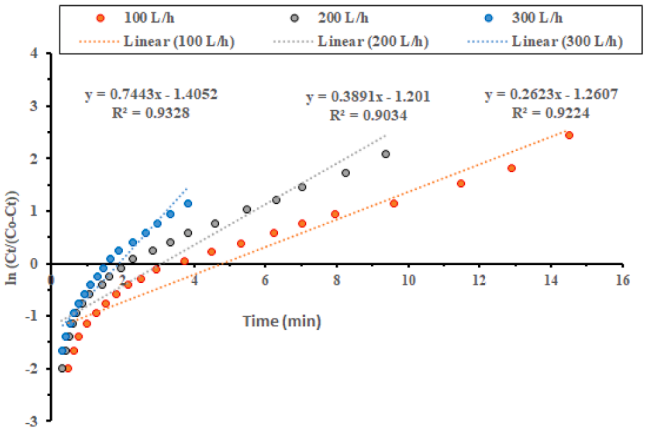

Fig. 11. Effect of Different Flowrate for Yoon Nelson Model PKSACX.

a wavenumber of 2950–2850 cm^{-1} was assigned to the stretching vibration of the C–H bond in the alkyl and aldehyde functional groups. Holocellulose and lignin are polymeric hydrocarbons composed of aliphatic and aromatic structures. The vibration caused by the stretching of the C—H bond was seen at a wavenumber of 2272.51 cm^{-1} for PKS, 2261.17 cm^{-1} for PKSAC, and in the range of 2251.64 to 2851.73 cm^{-1} was observed for the PKSACX. The PKS showed a C = C stretching functional group at a wavenumber of 1660 cm^{-1}, whereas the PKSAC displayed this functional group at 1630 cm^{-1}. The PKSACX, on the other hand, demonstrated a C = C stretching functional group at a precise wavenumber of 1616.98 cm^{-1}. The presence of aromatic compounds was suggested by peaks within the range of 1690–1450 cm^{-1}. The spectrogram was visually examined on the computer monitor,

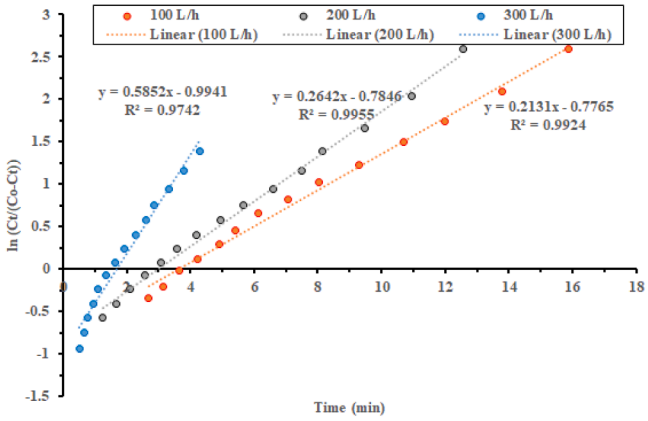

Fig. 12. Effect of Different Flowrate for Yoon Nelson Model PKSACXB.

displaying a graphical representation of the sample spectrogram [39].

3.1.4. *Thermogravimetric analysis*

Thermogravimetric Analysis (TGA) is done to determined thermal degradation of PKS, PKSAC, and PKSACX. TGA curves show that the pyrolysis of studied PKS, PKSAC, and PKSX is divided into four stages where it depicts the element content of moisture (%), volatile matter (%), ash (%), and fixed carbon (%) content [40]. In this case, the primary constituents of the biochar source, which is PKS, include moisture, cellulose, hemicellulose, and lignin. Fig. 3 shows the TGA black curve for PKS in the initial stage, where there's a mass loss of 11.92 % (equal to 1.1216 mg) until reaching 147.37 °C. This decrease in mass is the removal and elimination of moisture content from the PKS sample. Fig. 3 observes a mass reduction of 13.04 % (equivalent to 1.304 mg) during the initial stage of the TGA red curve for PKSAC, occurring around 145.61 °C. Fig. 3 shows a decrease in mass of 10.03 % (equivalent to 1.003 mg) during the first stage of the TGA green curve for PKSACX, occurring approximately at 146.17 °C. This mass reduction primarily arises from eliminating physically adsorbed water within the Xerogel, which is the key factor in this initial portion of the TGA curve. Effected of oxidizing atmosphere at 950 °C shows a mass loss of 63 %, compared to PKS. PKS Biochar also had more carbon, around 58.7 %, compared to Xerogel at 23.83 %. The peak at 950 °C represents carbon breakdown, and the remaining curve shows ash content. This significant loss might be due to the elimination of unstable components from PKS Biochar. Complete degradation of Xerogel Biochar happens at 1189.97 °C. The results are similar to previous studies [22].

3.2. *Adsorption test*

3.2.1. *Impact of gas flow rate on PKSSACXB, PKSACX, and their blended (PKSACXB) composites*

One of the most critical parameters to consider in an adsorption process is the gas flow rate due to its significant impact on adsorption

Table 4
Yoon- Nelson Adsorption Isotherm Model.

Type of Adsorbent	F(L/h)	W(g)	R^2	Slope	Interception at y-axis	Equation	K_{YN} (L/min.mg)	50 % Breakthrough Time τ
PKSAC	100	20 g	0.9909	0.3288	1.7873	$y = 0.3288x - 1.7873$	0.5508	4.540123
	200	20 g	0.9786	0.4424	1.3494	$y = 0.4424x - 1.3494$	0.6559	2.948468
	300	20 g	0.9729	0.7211	1.746	$y = 0.7211x - 1.746$	0.8743	1.732472
PKSACX	100	20 g	0.9224	0.2623	1.2607	$y = 0.2623x - 1.2607$	0.449	8.546102
	200	20 g	0.9034	0.3891	1.201	$y = 0.3891x - 1.201$	0.5849	6.449308
	300	20 g	0.9328	0.7443	1.4052	$y = 0.7443x - 1.4052$	0.9763	3.743419
PKSACXB	100	20 g	0.9955	0.2459	0.7819	$y = 0.2459x - 0.7819$	0.4868	4.218981
	200	20 g	0.9928	0.2696	0.8281	$y = 0.2696x - 0.8281$	0.5732	3.368632
	300	20 g	0.9742	0.5852	0.9941	$y = 0.5852x - 0.9941$	0.8522	2.459986

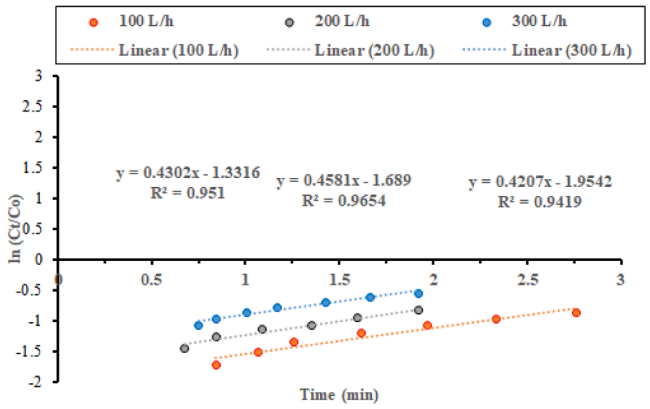

Fig. 13. Effect of Different Flowrate for Adams and Bohart Model PKSAC.

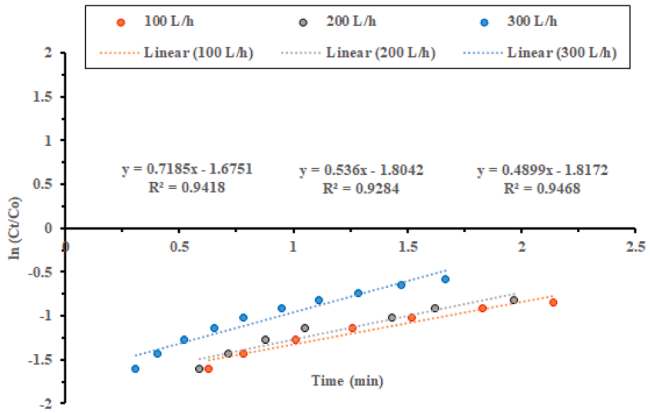

Fig. 14. Effect of Different Flowrate for Adams and Bohart Model PKSACX.

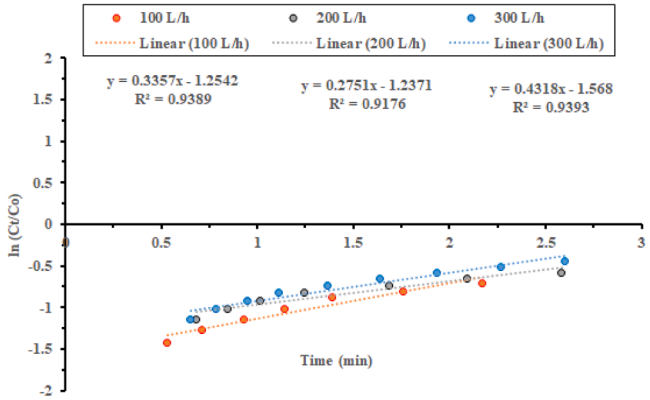

Fig. 15. Effect of Different Flowrate for Adams and Bohart Model PKSACXB.

capacity. Figs. 4, 5, and 6 show the exit concentration of gas over time, indicating that a slower flow rate allows more time for the adsorbent to reach its maximum adsorption capacity. This implies that higher flow rates reduce the retention period of SO_2 molecules on PKSACX in the packed bed system, thereby decreasing the system's adsorption capacity. Achieving higher adsorption capacities requires longer residence times [41] Therefore, it can be concluded that longer residence times at lower flow rates facilitate slower SO_2 diffusion, leading to a higher adsorption capacity.

3.3. Equilibrium studies

3.3.1. Thomas model

The experimental data were analyzed using the Thomas Model equation to determine the maximum adsorption capacity (q_0) and the kinetic coefficient (K_{TH}). The linear regression results and the corresponding R^2 values for both flow rates (100 L/h, 200 L/h and 300 L/h) are presented in Figs. 7, 8, and 9.

From the Figures Above, Higher flow rates decrease adsorption capacity, as faster flow rates leave less contact time between SO_2 and the adsorbent. Blended generally performs better in capacity than Xerogel and Activated carbon materials, especially at lower flow rates. These results align with the behavior predicted by the Thomas model, where the slope, intercept, and adsorption capacities vary with changes in gas flow rates [18].

We summarize the Thomas adsorption isotherm model for SO_2 adsorption using activated carbon, xerogel, and their blends at varying flow rates (F) in Table 3 activated carbon the adsorption capacity (q_o) decreases with increasing flow rate from 976.546 mg/g at 100 L/h to 703.364 mg/g at 300 L/h, reflecting reduced contact time. The (R^2) values (0.95–0.97) indicate a good model fit. Xerogel, the adsorption performance exhibits variability, with (q_o) peaking at 875.765 mg/g at 300 L/h. Lower (R^2) values (0.90–0.92) suggest a slightly weaker fit compared to activated carbon. Blended Adsorbents: Blends show consistent performance, with (q_o) increasing from 468.621 mg/g at 100 L/h to 928.391 mg/g at 300 L/h. The (R^2) values (0.96–0.97) confirm a strong model fit. Flow Rate Impact: across all adsorbents, the slope (K_{TH}) increases with flow rate, indicating faster SO_2 uptake at higher flows. However, high flow rates may limit contact time, affecting adsorption efficiency this study aligned with the study by [42].

3.3.2. Yoon Nelson model

The experimental data were also analyzed using the Yoon-Nelson Model equation by plotting the ln (Cf/(C0-Cf)) graph versus time. Figs. 10, 11, and 12 illustrate the effects of flow rate by using this model. The linear regression results from this graph can be used to determine the Yoon-Nelson proportionality constant (K_{YN}) and the time required to retain 50 % of the initial adsorbate (τ).

Figs. 10, 11, and 12, including the values of K_{TH}, q_0, and R^2. The figures indicate that as the flow rate increases, the value of K_{TH} increases while the value of q_0 decreases. The Thomas rate constant (K_{TH}) represents the time required for the adsorbent to reach full saturation, with a higher K_{TH} value indicating a shorter saturation period. On the other

Table 5
Shows the Adams and Bohart Adsorption Isotherm model.

Type of Adsorbent	F(L/h)	W(g)	R^2	Slope	Interception at y-axis	Equation	K_{AB} (L/mg)	N_o (mg/L)
PKSAC	100	20 g	0.9419	0.4207	1.9542	$y = 0.4207x - 1.9542$	0.005592	824.864
	200	20 g	0.9654	0.4581	1.689	$y = 0.4581x - 1.689$	0.015482	925.3943
	300	20 g	0.951	0.4302	1.3316	$y = 0.4302x - 1.3316$	0.012032	1155.324
PKSACX	100	20 g	0.9468	0.4899	1.8172	$y = 0.4899x - 1.8172$	0.010052	1047.997
	200	20 g	0.9284	0.536	1.8042	$y = 0.536x - 1.8042$	0.028132	1200.816
	300	20 g	0.9418	0.7185	1.6751	$y = 0.7185x - 1.6751$	0.0198	1660.14
PKSACXB	100	20 g	0.9393	0.4318	1.568	$y = 0.4318x - 1.568$	0.012908	1478.136
	200	20 g	0.9176	0.2751	1.2371	$y = 0.2751x - 1.2371$	0.028132	1749.519
	300	20 g	0.9389	0.3357	1.2542	$y = 0.3357x - 1.2542$	0.02173	2096.074

Table 6
Comparison of Isotherm Model in term of Correlation Coefficient.

Adsorbent	Flowrate (L/hr)	Isotherm Model	R^2
PKSAC	100	Thomas	0.9651
		Yoon-Nelson	0.9729
		Adam-Bohart	0.9419
	200	Thomas	0.9673
		Yoon-Nelson	0.9786
		Adam-Bohart	0.9654
	300	Thomas	0.9527
		Yoon-Nelson	0.9909
		Adam-Bohart	0.951
PKSACX	100	Thomas	0.9247
		Yoon-Nelson	0.9224
		Adam-Bohart	0.9468
	200	Thomas	0.9044
		Yoon-Nelson	0.9034
		Adam-Bohart	0.9284
	300	Thomas	0.9292
		Yoon-Nelson	0.9328
		Adam-Bohart	0.9418
PKSACXB	100	Thomas	0.9694
		Yoon-Nelson	0.9955
		Adam-Bohart	0.9393
	200	Thomas	0.9636
		Yoon-Nelson	0.9928
		Adam-Bohart	0.9176
	300	Thomas	0.9665
		Yoon-Nelson	0.9742
		Adam-Bohart	0.9389

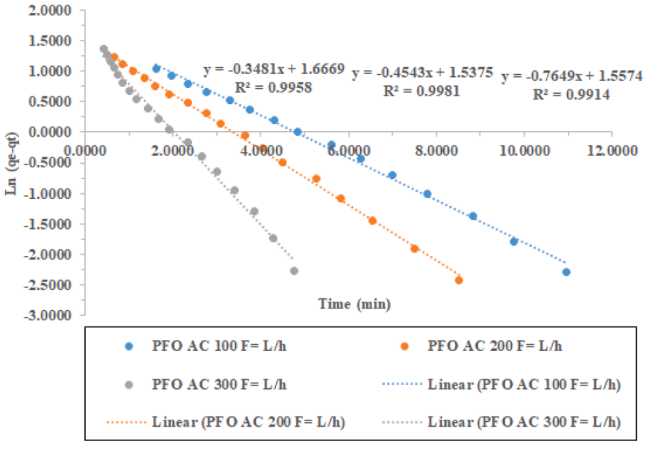

Fig. 16. Pseudo-first order (PKSAC) effect of flow rate.

hand, q_0 represents the maximum adsorption capacity, with a higher q_0 value indicating a greater amount of SO_2 adsorbed onto the adsorbent [43]. Thus, a higher flow rate results in the adsorbent reaching maximum saturation more quickly. However, reduced contact time between the adsorbent and the adsorbate leads to a lower adsorption

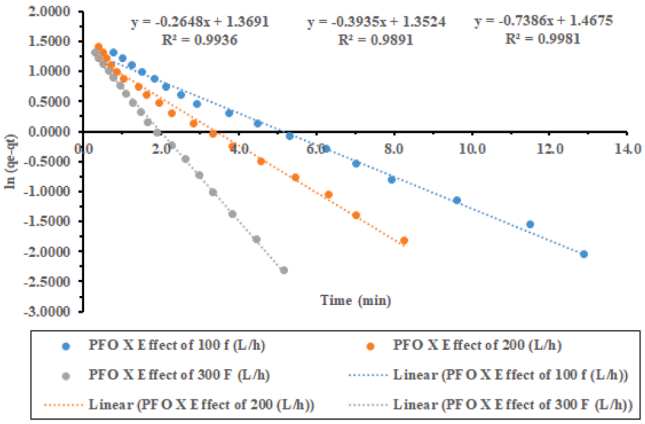

Fig. 17. Pseudo-First Order (PKSACX) effect of flow rate.

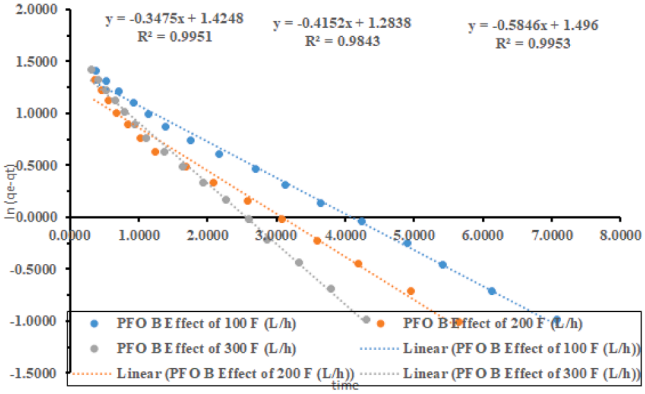

Fig. 18. Pseudo-First Order (PKSACXB) effect of flow rate.

capacity.

The Yoon-Nelson adsorption isotherm model results for SO_2 adsorption on activated carbon, xerogel, and their blends at varying flow rates (F) are presented in Table 4. Activated carbon's 50 % breakthrough time (τ) decreases significantly as the flow rate increases, from 4.54 min at 100 L/h to 1.73 min at 300 L/h, indicating faster adsorption. High (R^2) values (0.97–0.99) confirm a strong model fit. Xerogel's adsorption capacity shows moderate variability, with (τ) decreasing from 8.55 min at 100 L/h to 3.74 min at 300 L/h. The (R^2) values (0.90–0.93) are lower than those for activated carbon, reflecting a less robust fit. Blended Adsorbents, Blends exhibit balanced performance, with (τ) decreasing from 4.22 min at 100 L/h to 2.46 min at 300 L/h. Excellent (R^2) values (0.97–0.99) highlight the reliability of the model. Flow Rate Impact, across all adsorbents, the slope increases with flow rate, showing that adsorption occurs more rapidly at higher flows but with shorter breakthrough times. Our study is aligned with a study by [44,45].

Table 7
Pseudo-First Order Model Parameters.

Adsorbent	F (L/hr)	W	k_1	q_e	R^2	Slope	Intercept	Equations
PKSAC	100	20	1.1194883	4.0988236	0.9958	0.3481	1.6669	$y = -0.3481x + 1.6669$
	200	20	0.7404145	5.2809183	0.9981	0.4543	1.5375	$y = -0.4543x + 1.5375$
	300	20	1.1680816	5.1825644	0.9914	0.7649	1.5574	$y = -0.7649x + 1.5574$
PKSACX	100	20	0.5149508	3.6124998	0.9936	0.2648	1.3691	$y = -0.2648x + 1.3691$
	200	20	0.7510083	3.6513611	0.9891	0.3935	1.3524	$y = -0.3935x + 1.3524$
	300	20	1.1190277	3.3902376	0.9981	0.7386	1.4675	$y = -0.7386x + 1.4675$
PKSACXB	100	20	0.8670795	4.3732218	0.9969	0.3346	1.3949	$y = -0.3346x + 1.3949$
	200	20	1.0061807	3.7825561	0.9896	0.4369	1.3304	$y = -0.4369x + 1.3304$
	300	20	1.4257873	4.7355601	0.9968	0.5973	1.5126	$y = -0.5973x + 1.5126$

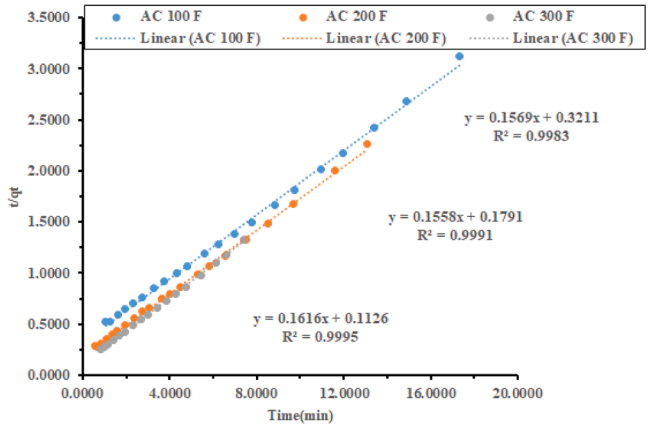

Fig. 19. Pseudo-Second Order PKSAC effect of flow rate.

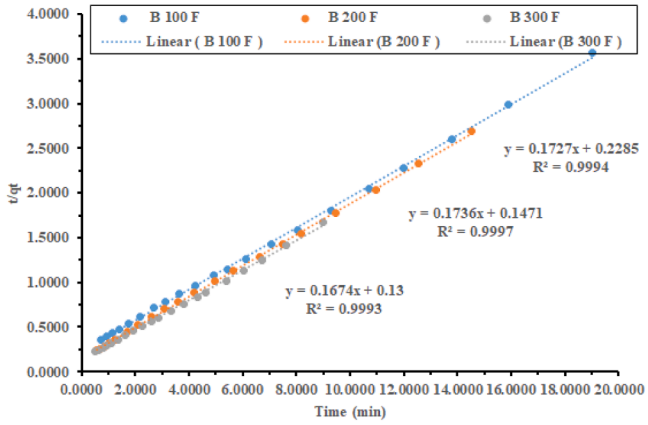

Fig. 21. Pseudo-Second Order PKSACXB effect of flow rate.

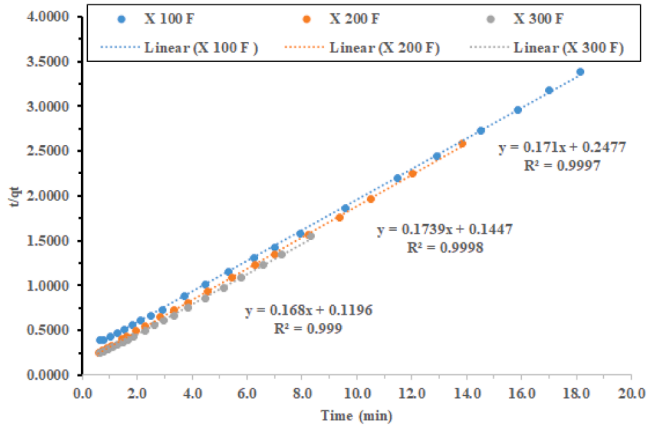

Fig. 20. Pseudo-Second Order PKSACX effect of flow rate.

3.3.3. Adam Bohart model

The data obtained from the adsorption test results were also analysed using the Adam-Bohart Model equation by plotting the graph of ln (C_f/C_0) versus time, as shown in Figs. 13, 14, and 15. This graph yields the regression results, allowing for determining the Adams-Bohart kinetics constant (K_{AB}) and the maximum volumetric sorption capacity (N_0).

Figs. 13, 14, and 15 summarize all the data and results obtained. It shows that as the flow rate increases, both K_{AB} and N0 values increase. Similar to the Thomas and Yoon-Nelson Model equations, higher kinetics constant (K_{AB}) values indicate that the adsorbent reaches saturation in a shorter period. The N0 values represent the maximum volumetric sorption capacity, showing similar results to the maximum adsorption capacity (q_0). However, the effect of flow rate differs as it is observed that higher flow rates result in a higher sorption capacity, which contrasts with the Thomas Model results where higher flow rates result in a lower maximum adsorption capacity.

To determine the most suitable model for representing the adsorption process, the R^2 values, which indicate the correlation and reliability of the models, must be compared. This comparison is shown in the Figures above. A higher R^2 value (closer to 1) indicates the model's higher correlation and reliability. For the effect of flow rate, the R^2 value for the Adam-Bohart model equation is significantly lower than those for the Thomas and Yoon-Nelson models, respectively. Therefore, due to their high R^2 values, the Thomas and Yoon-Nelson models are suitable for use. Based on these results, it can be concluded that the Thomas and Yoon-Nelson equations are the best modeling isotherms for the adsorption process.

Table 5 illustrates the results of the Adams and Bohart adsorption isotherm model for SO_2 adsorption on activated carbon, xerogel, and their blends at different flow rates (F). Activated Carbon, the adsorption capacity (N_o) increases with flow rate, peaking at 1155.324 mg/L at 300 L/h, indicating enhanced adsorption efficiency under faster flow conditions. The model shows a good fit (R^2) (0.94–0.97). Xerogel, a similar trend is observed, with (N_o) rising from 1047.997 mg/L at 100 L/h to 1660.14 mg/L at 300 L/h. The slightly lower (R^2) values (0.92–0.95) suggest a reasonably strong model fit. Blended Adsorbents, the blends demonstrate the highest (N_o) values, increasing from 1478.136 mg/L at 100 L/h to 2096.074 mg/L at 300 L/h, indicating superior adsorption performance. The (R^2) values (0.91–0.94) confirm a satisfactory fit. Flow Rate and Adsorption, across all adsorbents, the slope (K_{AB}) increases with flow rate, indicating faster adsorption kinetics. However, higher flow rates correlate with higher (N_o), suggesting improved capacity for SO_2 capture. Our study aligns with the findings reported in the research conducted by [46,47].

Table 6 evaluated the performance of different isotherm models—Thomas, Yoon-Nelson, and Adam-Bohart—across various flow rates (100, 200, and 300 L/hr) for three adsorbents: activated carbon, xerogel, and a blended adsorbent. The Yoon-Nelson model consistently shows the highest R^2 values across all adsorbents and flow rates,

Table 8
Pseudo-Second Order Model Parameters.

Adsorbent	F (L/hr)	W (g)	k_2	q_e	R^2	Slope	Intercept	Equation
PKSAC	100	20	0.29508514	6.55737705	0.9983	0.1569	0.3211	$y = 0.1569x + 0.3211$
	200	20	0.48643411	6.64010624	0.9991	0.1558	0.1791	$y = 0.1558x + 0.1791$
	300	20	0.78808933	6.29722922	0.9995	0.1616	0.1126	$y = 0.1616x + 0.1126$
PKSACX	100	20	0.69273967	5.79038796	0.9997	0.171	0.2477	$y = 0.171x + 0.2477$
	200	20	1.16655607	5.68828214	0.9998	0.1739	0.1447	$y = 0.1739x + 0.1447$
	300	20	1.42434211	5.77367206	0.999	0.168	0.1196	$y = 0.168x + 0.1196$
PKSACXB	100	20	0.74143167	5.85137507	0.9994	0.1727	0.2285	$y = 0.1727x + 0.2285$
	200	20	1.17241379	5.76701269	0.9997	0.1736	0.1471	$y = 0.1736x + 0.1471$
	300	20	1.2560241	5.99520384	0.9993	0.1674	0.13	$y = 0.1674x + 0.13$

indicating that it provides the best fit for the adsorption data. The Thomas model generally performs well, but its R^2 values are slightly lower than those of Yoon-Nelson. The Adam-Bohart model also shows good performance, with R^2 values close to those of the other models, but it typically ranks slightly lower. Overall, the Yoon-Nelson model is the most reliable for representing adsorption behaviour across different flow rates and adsorbent types.

3.4. Kinetic studies

3.4.1. Pseudo-First order

To study the kinetics of the adsorption process, the data were fitted into the pseudo-first-order kinetic equation, and a graph of Ln (qe-qt) versus time for the effect of flow rate was plotted, as shown in Figs. 16, 17, and 18.

This summarises the data and results extracted from Figs. 16, 17, and 18. The Figures indicate that higher flow rates result in less SO_2 adsorbed at equilibrium (q_e). This decrease in qe value with increased flow rates shown in Table 7 is likely due to the reduced contact time between the adsorbent and adsorbate at higher flow rates.

3.4.2. Pseudo-Second order

To study the kinetics of the adsorption process, the data were fitted into the pseudo-second-order kinetic equation, and a graph of (t/qt) versus time for the effect of flow rate was plotted, as shown in Figs. 19, 20, and 21.

Similar to the pseudo-first-order kinetics, the values of q_e and K_2 were obtained from the graphs (Figs. 19, 20, and 21) for the pseudo-second-order kinetics. The figures show the pseudo-first- and Pseudo order kinetics, which is higher flow rates result in a lower amount of SO_2 adsorbed at equilibrium (q_0). However, regarding the K_2 value, an increase in flow rate results in an increase in the K_2 value. To determine the most reliable kinetic model, the correlation and reliability (R^2) values have been compared. The summary of R^2 values for both parameters is shown in Figs. 16–21. In the comparison between pseudo-first-order and pseudo-second-order kinetics, the pseudo-first-order model shows higher R^2 values compared to the pseudo-second-order model, with values of 0.9994, 0.9997, and 0.9993 for flow rates of 100 L/h, 200 L/h, and 300 L/h, respectively. This, however, does not mean that the adsorption process only favors physisorption. Based on the R^2 values, we can infer that the adsorption process involves both physisorption and chemisorption. High R^2 values from both kinetic models indicate that both physisorption and chemisorption processes are likely present during adsorption. The Xerogel composition, as a solid with a liquid coating, supports the occurrence of both types of adsorption mechanisms [48]. Therefore, utilizing both the first-order and second-order kinetic equations can adequately capture the dynamics of adsorption in this system.

The kinetic parameters for SO_2 adsorption on PKSAC, PKSACX, and PKSACXB were determined by applying linear regression methods to several models. These included the pseudo-first-order and pseudo-second-order models on a heterogeneous surface. The goodness of fit for each model was evaluated using the coefficient of determination (R^2), providing insights into the most accurate representation of the adsorption kinetics [49]. Based on R^2 in Table 5 and R^2 in Table 8 values, the pseudo-second-order model best represents the adsorption kinetics for SO_2 on PKSAC, PKSACX, and PKSACXB.

4. Conclusion

This study explores a novel adsorbent for capturing SO_2 through adsorption, focusing on isotherm and kinetic models. The research examines the impact of flow rate and contact time on SO_2 adsorption using palm kernel shell-activated carbon and xerogel blends (PKSACXB). Sulphur dioxide (SO_2) is emitted into the atmosphere during the operation of coal-fired power plants, significantly harming the environment. SO_2 in flue gas can lead to respiratory issues and contribute to acid rain. As energy consumption increases, the amount of SO_2 released into the environment also rises. To address this pressing issue, palm kernel shell-activated carbon xerogel has proven to be an effective method for reducing SO_2 concentration in the air through the adsorption process. An equilibrium and kinetic study were carried out to investigate the adsorption of SO_2 onto PKSACXB comprehensively. The results indicated that the process favors a slower flow rate (100 L/h) to achieve higher adsorption. Additionally, the time required for the adsorbent to reach full saturation is longer at lower flow rates, as they provide extended contact time during the adsorption process. The study also inferred that, in terms of the effect of gas flow rate, the Thomas and Yoon-Nelson models are the best for modelling isotherms. For kinetic modelling, both the pseudo-first order and pseudo-second order models proved suitable, as they provided high correlation coefficient (R^2) values, which proves the adsorption process of sulfur dioxide achieved physical chemisorption. While physical adsorption is characterized by weak van der Waals forces and is generally reversible, chemisorption involves the formation of stronger chemical bonds, making it typically irreversible. The result also proved that the adsorption is physisorption and chemisorption because both the Pseudo-First Order and Pseudo-Second Order models exhibited a high correlation coefficient, making them suitable and compatible with the adsorption system.

CRediT authorship contribution statement

Ali Mohamed Saleh: Data curation, Conceptualization. **Azil Bahari Alias:** Funding acquisition, Formal analysis. **Syed Shatir A. Syed Hasan:** Methodology, Investigation. **Ali H. Jawad:** Resources, Project administration. **Thaer Abdulwahhab Shihab:** Software. **Obed M. Ali:** Supervision. **Wan Azlina Wan Ab Karim Ghani:** Validation. **Hadi Hamdi Mahdi:** Validation. **Noah Mohammed Saleh:** Visualization. **Omer Khalil Ahmed:** Writing – review & editing, Writing – original draft.

Declaration of competing interest

The authors declare that they have no known competing financial interests or personal relationships that could have appeared to influence the work reported in this paper.

Acknowledgment

The authors would like to express their deepest gratitude to all those who have provided the means and possibility for completing this work. The research was conducted at the School of Chemical Engineering, Universiti Teknologi MARA, Shah Alam, Selangor, Malaysia, under the support of the grant (600-TNCPI 5/3/DDF (KPK) (008/2023)).

Funding

No funding was received for this work.

Data availability

Data will be made available on request.

References

[1] S.A. Meo, N. Shaikh, M. Alotaibi, Association between air pollutants particulate matter (PM2. 5, PM10), nitrogen dioxide (NO2), sulfur dioxide (SO2), volatile organic compounds (VOCs), ground-level ozone (O3) and hypertension, J. King Saud Univ. 36 (2024) 103531.

[2] S. Nurhisanah, H. Hasyim, Environmental health risk assessment of sulfur dioxide (SO2) at workers around in combined cycle power plant (CCPP), Heliyon 8 (2022), https://doi.org/10.1016/j.heliyon.2022.e09388, 0–5.

[3] P. Saxena, S. Sonwani, Primary criteria air pollutants: environmental health effects BT - criteria air pollutants and their impact on environmental health, in: P. Saxena, S. Sonwani (Eds.), Springer Singapore, Singapore, 2019: pp. 49–82. https://doi.org/10.1007/978-981-13-9992-3_3.

[4] A. Grzywa-Celińska, A. Krusiński, J. Milanowski, Smoging kills'-effects of air pollution on human respiratory system, Ann. Agric. Environ. Med. 27 (2020) 1–5.

[5] S.H. Susetyo, A.U. Abidin, T. Nagaya, N. Kato, Y. Matsui, Environmental health risk assessment and acute effects of Sulfur Dioxide (SO2) inhalation exposure on traditional sulfur miners at Ijen Crater Volcano, Indonesia, Toxicol. Reports (2024) 101772.

[6] A. Islam, S.H. Teo, C.H. Ng, Y.H. Taufiq-Yap, S.Y.T. Choong, M.R. Awual, Progress in recent sustainable materials for greenhouse gas (NOx and SOx) emission mitigation, Prog. Mater. Sci. 132 (2023) 101033, https://doi.org/10.1016/j.pmatsci.2022.101033.

[7] P. Kumar, A.B. Singh, T. Arora, S. Singh, R. Singh, Critical review on emerging health effects associated with the indoor air quality and its sustainable management, Sci. Total Environ. 872 (2023) 162163.

[8] H.-M. Liu, H.-H. Li, Y. Yao, J.-J. Wang, L. Mi, Application status of dry desulfurization in industrial waste gas treatment, 111 (2017) 130–133. https://doi.org/10.2991/icsd-17.2017.20.

[9] A.M. Saleh, N.M. Saleh, Production of biofuels from biomass as an approach towards sustainable development: a short review, 3 (2022) 9–21.

[10] A. Mohammed, S. Azil, B. Alias, H.H. Mahdi, A.H. Jawad, S.S. A., N.M. Saleh, O.K. Ahmed, A.M. Saleh, Characterizing biochar derived from palm kernel shell biomass via slow pyrolysis for adsorption applications, 6 (2024) 10–20.

[11] N.D. Hutson, R.T. Yang, Theoretical basis for the Dubinin-Radushkevitch (DR) adsorption isotherm equation, Adsorption 3 (1997) 189–195.

[12] É.C. Lima, M.A. Adebayo, F.M. Machado, Kinetic and equilibrium models of adsorption BT - carbon nanomaterials as adsorbents for environmental and biological applications, in: C.P. Bergmann, F.M. Machado (Eds.), Springer International Publishing, Cham, 2015: pp. 33–69. https://doi.org/10.1007/978-3-319-18875-1_3.

[13] B. Li, Q. Zhang, C. Ma, Kinetics of SO2 adsorption on powder activated carbon in a drop tube furnace, Int. J. Chem. Eng. 2021 (2021), https://doi.org/10.1155/2021/8886646.

[14] H. Zare Aliabad, S. Mirzaei, Removal of CO2 and H2S using aqueous alkanolamine solutions, World Acad. Sci. Eng. Technol. 49 (2009) 194–203.

[15] L. Lü, D. Lu, L. Chen, F. Luo, Removal of Cd (II) by modified lawny grass cellulose adsorbent, Desalination 259 (2010) 120–130.

[16] X. Li, J. Han, Y. Liu, Z. Dou, T. Zhang, Summary of research progress on industrial flue gas desulfurization technology, Sep. Purif. Technol. 281 (2022) 119849.

[17] D. Qarizada, N.M.R. Noraini, A.B. Alias, M.F. Fadil, H. Kambakhsh, Equilibrium isotherms and adsorption kinetics models of hydrogen sulphide using xerogel adsorbent derives from palm kernel shell biochar, Int. J. Eng. Adv. Res. 4 (2022) 16–33. http://myjms.mohe.gov.my/index.php/ijearJournalwebsite:http://myjms.mohe.gov.my/index.php/ijearhttp://myjms.mohe.gov.my/index.php/ijear.

[18] A.M. Saleh, H.H. Mahdi, A.B. Alias, N.K.A. Hadi, D. Qarizada, A.H. Jawad, N. M. Saleh, Equilibrium and kinetic studies in adsorption of H2S using coconut shell activated carbon xerogel: effect of mass adsorbent and temperature, Desalin. Water Treat. (2024) 100149, https://doi.org/10.1016/j.dwt.2024.100149.

[19] A.M. Saleh, H.H. Mahdi, A.B. Alias, O.M. Ali, W.A.W. Ab Karim Ghani, T.A. Shihab, S.S.A. Syed Hasan, O.K. Ahmed, N.M. Saleh, Application of response surface methodology (rsm) for optimization of hydrogen sulphide adsorption using coconut shell activated carbon xerogel: effect of adsorption pressure and hydrogen sulphide flowrate, Ann. Chim. Sci. Des Mater. 48 (2024) 509–518, https://doi.org/10.18280/acsm.480408.

[20] K. Kaur, R. Kaur, H. Kaur, A systematic review of lignocellulosic biomass for remediation of environmental pollutants, Appl. Surf. Sci. Adv. 19 (2024) 100547, https://doi.org/10.1016/j.apsadv.2023.100547.

[21] H. Ning, R. Tang, C. Li, X. Gu, Z. Gong, C. Zhu, J. Li, K. Wang, J. Yu, Recent advances in process and materials for dry desulfurization of industrial flue gas: an overview, Sep. Purif. Technol. (2024) 128425.

[22] H.H. Mahdi, A.M. Saleh, A.B. Alias, A.H. Jawad, S.D. Salman, M.M. Mostafa, D. Qarizada, N.M. Saleh, M. Abdulqader, Synthesis and characterization of xerogel derived from palm kernel shell biochar and comparison with commercial activated carbon, J. Ecol. Eng. (2024). http://www.jeeng.net/Synthesis-and-Characterization-of-xerogel-Derived-from-Palm-Kernel-Shell-Biochar,183719,0,2.html.

[23] V.S. Bhandari, S.H. Kulkarni, Optimization of heat sink for thyristor using particle swarm optimization, Results Eng 4 (2019) 100034, https://doi.org/10.1016/j.rineng.2019.100034.

[24] T.S. Dhahi, A.K. Yousif Dafhalla, A.W. Al-Mufti, M.E. Elobaid, T. Adam, S.C. B. Gopinath, Application of Nanobiosensor engineering in the diagnosis of neurodegenerative disorders, Results Eng. 24 (2024) 102790, https://doi.org/10.1016/j.rineng.2024.102790.

[25] A.R. AlBajalan, A.A. Rasol, M.N.A.M. Norddin, J.O. Oseh, M.N. Yahya, O.S. Ikenna, Applying graphene oxide Nanosheets(GONSs) in WBM to enhance its properties and well bore stability: a literature review, Results Eng. 24 (2024) 103015, https://doi.org/10.1016/j.rineng.2024.103015.

[26] M.S. Tovar-Oliva, I. Tudela, Electrodeposition of nano- and micro-materials: advancements in electrocatalysts for electrochemical applications, Results Eng 24 (2024) 103285, https://doi.org/10.1016/j.rineng.2024.103285.

[27] H. Zentou, M. Aliyu, M.A. Abdalla, O.Y. Abdelaziz, B. Hoque, A.M. Alloush, I. M. Tayeb, K. Patchigolla, M.M. Abdelnaby, Advancements and challenges in adsorption-based carbon capture technology: from fundamentals to deployment, Chem. Rec. (2024) e202400188.

[28] N.M.R. Noraini, A.B. Alias, D. Qarizada, F.A.M. Azman, Z.A. Rashid, M.R.C. Hasan, Synthesis and characterization of xerogel from palm kernel shell biochar, (2022).

[29] N.M.R. Noraini, A.B.A. Alias, D. Qarizada, F.A. Md Azman, Z. Abdul Rashid, M. R. Che Hasan, Synthesis and characterization of xerogel from Palm Kernel Shell Biochar, J. Mech. Eng. 11 (2022) 211–226.

[30] C. Quan, Y. Zhou, C. Wu, G. Xu, D. Feng, Y. Zhang, N. Gao, Valorization of solid digestate into activated carbon and its potential for CO2 capture, J. Anal. Appl. Pyrolysis 169 (2023) 105874, https://doi.org/10.1016/j.jaap.2023.105874.

[31] K.F.Y. Hadi Hamdi Mahdi, Ali Mohammed Saleh, Azil Bahari Alias, Obed M. Ali, Wan Azlina Wan Ab Karim Ghani, Thaer Abdulwahhab Shihab5, Noah Mohammed Saleh, Optimization for the effects of coconut shell activated carbon xerogel weight and temperature on the hydrogen sulphide adsorption using response surface methodology, Int. J. Energy Convers. 12 (2024).

[32] A.M. Saleh, H.H. Mahdi, A.B. Alias, N.K.A. Hadi, D. Qarizada, A.H. Jawad, N. M. Saleh, Equilibrium and kinetic studies in adsorption of H2S using coconut shell activated carbon xerogel: effect of mass adsorbent and temperature, Desalin. Water Treat. 317 (2024) 100149, https://doi.org/10.1016/j.dwt.2024.100149.

[33] N.M.S. Ali Mohammed saleh, Hadi Hamdi Mahdi, Obed Mojeed Ali, Azil Bahari Alias, No title optimization for the effects of coconut shell activated carbon Xerogel weight and temperature on the Hydrogen Sulphide adsorption using response surface methodology, Int. J. Energy Convers. 12 (2024) 150–158, https://doi.org/10.15866/irecon.v12i4.25011.

[34] T.A. Saleh, Isotherm models of adsorption processes on adsorbents and nanoadsorbents. Interface Sci. Technol., Elsevier, 2022, pp. 99–126.

[35] J. Cruz-Olivares, C. Pérez-Alonso, G. Martínez-Barrera, G. Roa-Morales, G. López-Téllez, E.M. del Campo-López, Modeling and scaling up of the Cr (VI) adsorption process by using mexicalcite natural mineral in a packed bed column, Results Eng 16 (2022) 100687.

[36] E.D. Revellame, D.L. Fortela, W. Sharp, R. Hernandez, M.E. Zappi, Adsorption kinetic modeling using pseudo-first order and pseudo-second order rate laws: a review, Clean. Eng. Technol. 1 (2020) 100032.

[37] A.N. Mustapa, Á. Martín, M.J. Cocero, Alginate aerogels dried by supercritical CO2 as herbal delivery carrier, Malays. J. Anal. Sci 22 (2018) 522–531.

[38] N.M.R. Noraini, A.B. Alias, D. Qarizada, F.A.M. Azman, Z.A. Rashid, M.R.C. Hasan, Synthesis and characterization of Xerogel from Palm Kernel shell biochar, J. Mech. Eng. 11 (2022) 211–226.

[39] P.E. Imoisili, K.O. Ukoba, T.-C. Jen, Synthesis and characterization of amorphous mesoporous silica from palm kernel shell ash, Boletín La Soc. Española Cerámica y Vidr 59 (2020) 159–164.

[40] P.E. Imoisili, K.O. Ukoba, T.-C. Jen, Green technology extraction and characterisation of silica nanoparticles from palm kernel shell ash via sol–gel, J. Mater. Res. Technol. 9 (2020) 307–313.

[41] K.O. Yoro, M.K. Amosa, P.T. Sekoai, M.O. Daramola, Modelling and experimental investigation of effects of moisture and operating parameters during the adsorption of CO 2 onto polyaspartamide, Int. J. Coal Sci. Technol. 6 (2019) 225–234.

[42] F. Gritti, G. Guiochon, Effect of the flow rate on the measurement of adsorption data by dynamic frontal analysis, J. Chromatogr. A 1069 (2005) 31–42, https://doi.org/10.1016/j.chroma.2004.08.129.

[43] O.B. Omitola, M.N. Abonyi, K.G. Akpomie, F.A. Dawodu, Adams-Bohart, Yoon-Nelson, and Thomas modeling of the fix-bed continuous column adsorption of amoxicillin onto silver nanoparticle-maize leaf composite, Appl. Water Sci. 12 (2022) 94.

[44] D.T. Mekonnen, E. Alemayehu, B. Lennartz, Fixed-bed column technique for the removal of phosphate from water using leftover coal, Materials (Basel) 14 (2021), https://doi.org/10.3390/ma14195466.

[45] E. Salehi, M. Yarali, A. Ebadi Amooghin, Comparison of adsorption properties of activated carbons with different crops residues as precursors for gold cyanide recovery: an iranian gold industry guide, Iran. J. Chem. Chem. Eng. 39 (2020) 213–229.
[46] O.A. Habeeb, K. Ramesh, G.A.M. Ali, Roslibin Mohd Yunus, Low-cost and eco-friendly activated carbon from modified palm kernel shell for hydrogen sulfide removal from wastewater: adsorption and kinetic studies, Desalin. Water Treat. 84 (2017) 205–214, https://doi.org/10.5004/dwt.2017.21196.
[47] S. Sumathi, S. Bhatia, K.T. Lee, A.R. Mohamed, Adsorption isotherm models and properties of SO2 and NO removal by palm shell activated carbon supported with cerium (Ce/PSAC), Chem. Eng. J. 162 (2010) 194–200, https://doi.org/10.1016/j.cej.2010.05.028.
[48] A.A. Abd Rahman*, A.B. Alias, M.A.A. Hamzah, M. Aidil Ali, Adsorption kinetics and equilibrium isotherms modeling of h2s on hydrogel biochar and biochar adsorbent from rice husk, Int. J. Recent Technol. Eng. 8 (2019) 6871–6878, https://doi.org/10.35940/ijrte.d5208.118419.
[49] A.M. Kisiela-Czajka, B. Dziejarski, Linear and non-linear regression analysis for the adsorption kinetics of so2 in a fixed carbon bed reactor—a case study, Energies 15 (2022), https://doi.org/10.3390/en15020633.